Journal of Physics: Conference Series **318** (2011) 052027 doi:10.1088/1742-6596/318/5/052027

Turbulence induced lift experienced by large particles in a turbulent flow

Robert Zimmermann[1] & Yoann Gasteuil[1] & Romain Volk[1] & Mickaël Bourgoin[2] & Alain Pumir[1] & Jean-François Pinton[1]

International Collaboration for Turbulence Research
[1], Laboratoire de Physique, ENS Lyon, France
[2], LEGI Grenoble, France

E-mail: robert.zimmermann@ens-lyon.fr

Abstract. The translation and rotation of a large, neutrally buoyant, particle, freely advected by a turbulent flow is determined experimentally. We observe that, both, the orientation the angular velocity with respect to the trajectory and the translational acceleration conditioned on the spinning velocity provides evidence of a lift force, $\boldsymbol{F}_{\rm lift} \propto \boldsymbol{\omega} \times \boldsymbol{v}_{\rm rel}$, acting on the particle. New results of the dynamics of the coupling between the particle's rotation and its translation are presented.

The description of a solid object freely advected in a fluid requires, in addition to its 3 translational degrees of freedom characterizing its position, 3 rotational degrees of freedom, specifying its orientation with respect to a reference frame. According to Newton's laws, the evolution of its position and of its orientation depends on the forces and torques acting on the particle at each instant, which result from the interaction between the object and the turbulent flow. Their experimental determination raises challenging issues as one needs to follow the object with a very good temporal and spatial resolution for a precise measurement.

For spherical particles which are much smaller than the smallest length scale of the flow the problem has be solved to a large extent (Gatignol (1983); Maxey & Riley (1983)) : rotation and translation decouple in the stokes limit and no back reaction from the rotational motion affects its translation. However, for particles larger than the smallest length scale of the flow, a full derivation of the equation of motion is still not available and the quantification of a lift force is under debate.

The possible existence of such a force has been the subject of several studies (Loth & Dorgan (2009); Auton *et al.* (1988)). It can be viewed as a generalization of the Magnus force, derived in an inviscid, laminar flow: $\boldsymbol{F}_{\rm lift} = C_{\rm lift}\, \boldsymbol{\omega} \times \boldsymbol{v}_{\rm rel}$, where $\boldsymbol{\omega}$ and $\boldsymbol{v}_{\rm rel}$ are the rotation of the particle in the flow and the slip velocity between the fluid and particle, respectively. A lift force has been observed in laboratory experiments, when the flow is steady and laminar (van Nierop *et al.* (2007); Rastello *et al.* (2009)), the flow conditions in these experiments are clearly very different from the case of a particle moving in a turbulent flow.

Here, we measure simultaneously the translational and rotational motion of a neutrally buoyant spherical particle, whose diameter is a fraction of the integral size of the turbulence. Then we report experimental data on the dynamics of the particle and show evidence of a lift force coupling the rotational and translational dynamics.

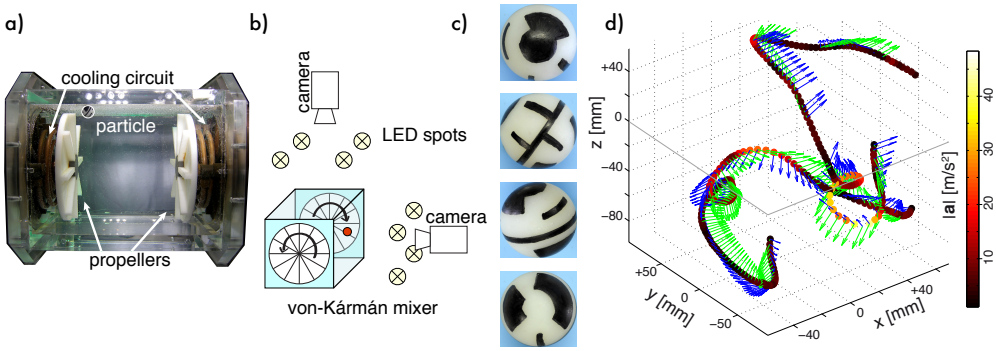

Figure 1. (a) The flow domain in between the impeller is a box of width $H = 20$ cm; the disks have diameter $2R = 19$ cm, fitted with straight blades 1 cm in height; (b) It is illuminated by high power LEDs and sequences of gray scale images are recorded using high-speed cameras; (c) an adequate texture painted on the particle allows the tracking of its orientation; (d) Example of particle tracks and orientations (the green and blue arrows mark North-South and East-West directions).

1. Setup & Technique

The measurements reported here use the same flow and tracking technique as in Zimmermann *et al.* (2011*b*,*a*). The fluid fills a plexiglass cylinder with square basis of width $H = 20$ cm and length 30 cm (Fig. 1(a)). The flow is driven by two counter rotating discs of diameter $2R = 19$ cm fitted with straight blades to ensure an inertial steering of the fluid. The distance between the discs is $H = 20$ cm and the rotation rate of the discs is fixed at $\Omega = 3$ Hz with two calibrated DC motors so that the discs rotate at same rotation rate but with opposite directions.

This type of turbulence generator is able to produce a highly turbulent flow and is widely used both for Eulerian and Lagrangian turbulence measurements (cf Toschi & Bodenschatz (2009)). Unfortunately the produced turbulent flow can be considered to be isotropic and homogeneous only in the vicinity of its geometrical center.

In the following, we study the dynamics of a homogeneous PolyAmide sphere of diameter $D = 18$ mm freely advected in the turbulent flow. As the density of sphere is $\rho_p = 1140$ kg.m^{-3}, we adjust the density of the fluid to that of the sphere by adding glycerol to the water. The resulting viscosity of the mixture is $\nu = 8.5\ 10^{-6}$ m^2.s^{-1} measured at 20° C, the temperature at which the flow is regulated by a cold water circulation behind the discs. The sphere's size is comparable to the integral size of the flow and we record its motion at a frequency of 600 Hz with 2 high-speed video cameras (Phantom v12, Vision Research) in a rather large volume covering 75% of the radial and axial distances on either side of the flow center.
The position of the sphere is then determined using a position tracking algorithm. The time-resolved determination of the absolute orientation of the sphere (Zimmermann *et al.* (2011*b*)) is carried out by painting a pattern that enables a determination of the particle's orientation from the camera images, cf. Fig. 1(c). A few sample trajectories are shown in Fig. 1(d), showing both the position, color coded for the amplitude of the acceleration, together with two vectors fixed in the reference frame of the particle.

2. Results

In the results reported here, the driving disks are rotated at 3 Hz, which corresponds to an energy

injection rate of $\epsilon \approx 1.7$ W.kg^{-1}. The Kolmogorov scales are then estimated to $\eta \sim 140$ μm and $\tau_\eta \sim 2.2$ ms, whereas the integral scales are $L_{\text{int}} \sim 3$ cm and $T_{\text{int}} \sim 0.3$ s. The particle size compares as $D/\eta \sim 130$ and $D/L_{\text{int}} \sim 0.6$. The Reynolds number based on the particle is 1200 ± 400 and reaches values up to 4000. The Reynolds number based on the Taylor micro-scale is estimated as $Re_\lambda = 200 \pm 50$. It should be noted that most trajectories span over a volume which cannot be considered to be homogeneous and isotropic but is rather dominated by the large scale dynamics of the von-Kármán flow.

Table 1. Characteristic values (mean ± rms) of the particle motion.

		x	y	z	Norm
$\boldsymbol{v}$	$[m/s]$	0 ± 0.28	0 ± 0.40	0 ± 0.37	0.6 ± 0.2
$\boldsymbol{a}$	$[m/s^2]$	-0.2 ± 5.6	-0.3 ± 5.8	0.2 ± 6.3	8.5 ± 5.6
$\boldsymbol{\omega}$	$[rad/s]$	0 ± 6.5	-0.2 ± 7.8	-0.1 ± 7.8	11.6 ± 5.5
$\boldsymbol{\alpha}$	$[rad/s^2]$	0 ± 510	0 ± 440	0 ± 460	670 ± 580
Energy, Translation	$[J]$	$E_{trans} = \frac{m}{2}\boldsymbol{v}^2 = (650 \pm 460)\ 10^{-6}$			
Energy, Rotation	$[J]$	$E_{rot} = \frac{J}{2}\boldsymbol{\omega}^2 = (9.23 \pm 9.63)\ 10^{-6}$			
energy transfer rate	$[m^2.s^{-3}]$	$\langle \boldsymbol{v} \cdot \boldsymbol{a} \rangle = -0.4 \pm 3.1\ \ m^2.s^{-3}$			
Power	$[mW]$	$\frac{d}{dt}\left(E_{rot} + E_{trans}\right) = -1.4 \pm 23$			

2.1. Dynamics & Energy of the Particle

A summary of particle motion is provided in table 1. The velocities are similar in y and z direction however they differ from the x direction. This is due to the fact that x is the direction of the axis of the impellers.

Despite the large particle size, both, the translational and angular accelerations exhibit very wide probability distributions, a manifestation of intermittency.

Fig. 2a shows the PDF of the translation as well as the rotation energy. One observes that the rotation energy $E_{rot} = \frac{J}{2}\boldsymbol{\omega}^2$ is approximately 50 times smaller than the energy associated to the translation $E_{trans} = \frac{m}{2}\boldsymbol{v}^2$. This agrees with the PDF of the ratio $\frac{E_{rot}}{E_{rot}+E_{trans}}$ displayed in Fig. 2b: contributions of more than 10% of E_{rot} to the total kinetic energy are strongly unlikely. If we estimate the relative magnitude of the mean rotation energy and kinetic (translational) energy we get

$$\frac{E_{trans}}{E_{rot}} = \frac{\frac{1}{2} m\, \boldsymbol{v}^2}{\frac{1}{2}\left(\frac{2}{5} m\, r^2\right)\, \boldsymbol{\omega}^2} = \frac{5}{2}\left(\frac{|\boldsymbol{v}|}{r\ |\boldsymbol{\omega}|}\right)^2 \tag{1}$$

We found (cf table 1) $\|\boldsymbol{v}\| = 0.6 m/s$ and $|\boldsymbol{\omega}| \approx 12\ rad/s$ ($r \cdot |\boldsymbol{\omega}| \approx 0.12 m/s$), *i.e.* the rotational energy, E_{rot}, is about 60 times smaller than the translational energy, E_{trans}. The estimates of the energy above do not take into account the fluid motion; including the entrained fluid would lead to a stronger relative contribution of rotation. According to numerical simulations by Naso & Prosperetti (2010) the particle entrains the fluids up to a distance of 2 particle diameter, D. At this value it is $\frac{E_{trans}}{E_{rot}(2\,D)} = 5$. A recent experimental development by Gibert *et al.* (2011) which follows tracer particles and rigid gel spheres simultaneously is expected to give further insights on the interaction of the particle with its surrounding fluid.

We also investigated the auto correlation of both parts of the kinetic energy. In contrast to the translation the auto-correlation of E_{rot} shows 2 different time scales. Similar behavior has be observed in jets for the vorticity of the flow measured with acoustical scattering (Mazellier (2005)).

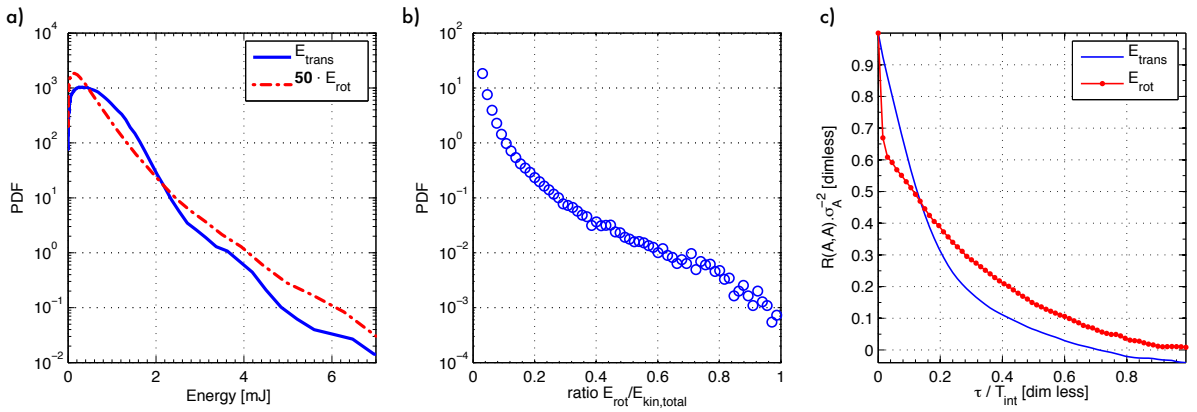

Figure 2. a) PDF of $E_{trans} = \frac{m}{2}\boldsymbol{v}^2$ and $E_{rot} = \frac{J}{2}\boldsymbol{\omega}^2$, note that $\mathbf{50} \times E_{rot}$ is compared to E_{trans} **b)** contribution of the roation energy, E_{rot}, to the total kinetic energy, $E_{rot} + E_{trans}$ **c)** Auto correlation of E_{rot} and E_{trans}

2.2. Lift Force

The Frenet formulas define a local coordinate system (CS) which is attached to and moving with the trajectory:

$$\boldsymbol{T}(t) = \frac{\dot{\boldsymbol{r}}(t)}{\|\dot{\boldsymbol{r}}(t)\|} \quad , \quad \boldsymbol{N}(t) = \boldsymbol{B}(t) \times \boldsymbol{T}(t) \quad \text{and} \quad \boldsymbol{B}(t) = \frac{\dot{\boldsymbol{r}} \times \ddot{\boldsymbol{r}}}{\|\dot{\boldsymbol{r}} \times \ddot{\boldsymbol{r}}\|} \tag{2}$$

with $\boldsymbol{r} = \boldsymbol{r}(t)$ the position of the particle at time t. $\boldsymbol{T}$, $\boldsymbol{N}$, $\boldsymbol{B}$ are the so-called tangent, normal, and binormal unit vectors defining the coordinate system. Fig. 3a depicts a sketch of the Frenet CS defined by the trajectory.

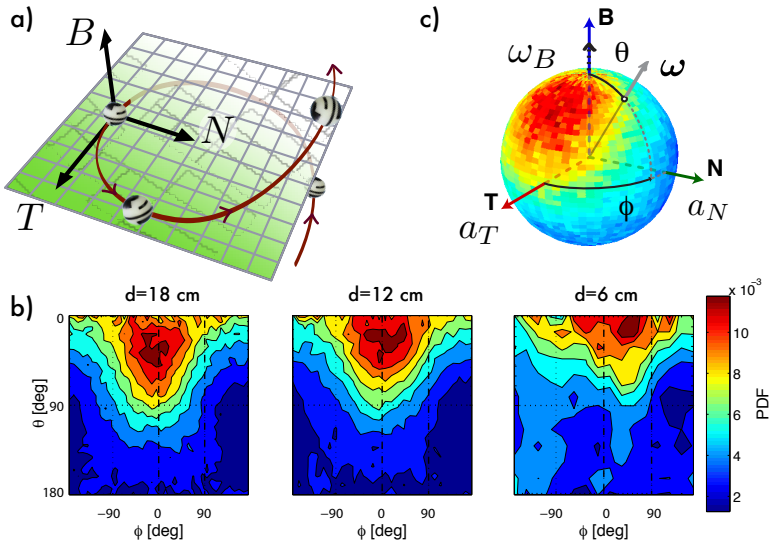

Figure 3. **a)** the comoving Frenet coordinate system as defined by the trajectory; by construction all forces are in the $(\boldsymbol{T} - \boldsymbol{N})-$plane **b)** Probability of the direction of $\boldsymbol{\omega}$ with respect to the ($\boldsymbol{T}$, $\boldsymbol{N}$, $\boldsymbol{B}$) reference frame using the full observation volume ($d = 18cm$) as well as two smaller regions in the center, **c)** sketch of the mapping of $\boldsymbol{\omega}$ to the Frenet CS, its texture is a rendering of the PDF shown in Fig. 3a

It is worthwhile to express the acceleration $\boldsymbol{a}$ and velocity $\boldsymbol{v}$ of the particle in this particular CS. One obtains $\boldsymbol{v} = \|\boldsymbol{v}\|\,\boldsymbol{T}$ and

$$\boldsymbol{a}(t) = \frac{d}{dt}\boldsymbol{v} = \left(\frac{d}{dt}\|\boldsymbol{v}\|\right)\boldsymbol{T} + \frac{1}{\rho(t)}\|\boldsymbol{v}(t)\|^2\,\boldsymbol{N} = a_T\boldsymbol{T} + a_N\boldsymbol{N} \quad , \tag{3}$$

where $\kappa(t) \equiv \frac{1}{\rho(t)}$ is the curvature of the trajectory and a_N is the well known centrifugal acceleration. In other words, the acceleration vector lies in the $(\boldsymbol{T}-\boldsymbol{N})-$plane and the velocity is always parallel with $\boldsymbol{T}$. We, therefore, note that a lift force of the form $\boldsymbol{F}_{\text{lift}} = C_{\text{lift}}\,\boldsymbol{\omega}\times\boldsymbol{v}_{\text{rel}}$, which is perpendicular to v_{rel}, can only contribute to a_N. Unfortunately, our measurement technique can not measure the flow around the particle and we cannot access the relative velocity, $\boldsymbol{v}_{\text{rel}}$, but only its absolute velocity, $\boldsymbol{v}$.

To check for an alignment of the angular velocity to the trajectory one can express the direction of ω in the ($\boldsymbol{T}$, $\boldsymbol{N}$, $\boldsymbol{B}$) frame by spherical coordinates (ϕ, θ) as sketched in Fig. 3c). The two-dimensional probability density function(PDF) of the direction of $\boldsymbol{\omega}$ is depicted in Fig. 3b) for 3 measurement volumes[1]. A three-dimensional visualization is provided in Fig. 3c.

In the following we define $\omega_B \equiv \boldsymbol{\omega}\cdot\boldsymbol{B}$: we find that $\langle\omega_B\rangle > 0$, with the peak of the PDF being at $\theta \approx 30°$. By construction it is $\boldsymbol{v} = |\boldsymbol{v}|\cdot\boldsymbol{T}$ and $\boldsymbol{B}\times\boldsymbol{T} = \boldsymbol{N}$, therefore $\langle\omega_B\rangle > 0$ implies that the parameter C_{lift} of the lift force is positive.

Moreover, $\boldsymbol{\omega}$ is aligned perpendicular to $\boldsymbol{N}$. Consequently, $\boldsymbol{\omega}\times\boldsymbol{v}$ lies in the $(\boldsymbol{T},\boldsymbol{N})$-plane and is parallel with $\boldsymbol{N}$. This observation is consistent with a Magnus force $a_{\text{lift}}\times\boldsymbol{N}$; however, the fairly sharp distribution of the direction of $\boldsymbol{\omega}$ on the sphere is remarkable.

The von-Kármán flow is known for its large scale inhomogeneities (cf Ouellette *et al.* (2006)). Therefore, we verified our observations by using only data points within a box of edge length d in the center (cf. the middle and right plot in Fig. 3b). Despite a significant reduction in the amount of data we find that preferential alignment is robust and not an artifact of the large scale flow of the apparatus. Fig. 2c shows that the kinetic energy uncorrelates in less than $\frac{1}{2}T_{\text{int}}$. Within this time the particle moved about $9cm$ along its (non-straight) trajectory. Thus, for the smaller observation volumes the particle lost all possible trace of the impellers and *e.g.* possible contact with them.

The lift force $\boldsymbol{F}_{\text{lift}} \propto \boldsymbol{\omega}\times\boldsymbol{v}$ expressed in the Frenet CS suggests a contribution of $|\boldsymbol{v}|\times\omega_B$ to the acceleration(*i.e.* force), a_N. Fig. 4a shows the amplitude of the acceleration, a_N, conditioned on the amplitude of ω_B. The averaged normal acceleration conditioned on ω_B increases by 50% from 6 to 9 m/s^2 when the particle rotation varies in the range ± 2 Hz ($= 12$ rad/s). The effect is stronger if ω_B is positive, however, this observation might be biased due to the fact that much less data is available for $\omega_B < 0$ (cf Fig. 3b).

Fig. 4a further shows that restricting the data to smaller regions in the center of the apparatus, shows that the dependence of a_N on ω_B does not depend on the large scale mean flow of the apparatus.

We now focus on the dynamics of the coupling. The cross correlation $R(a_N, |\boldsymbol{v}|\times\omega_B)$ is provided in Fig. 4b. The peak is at $+18$ ms, which corresponds to a few Kolmogorov time scales, τ_η. It also equals 11 frames of the cameras, *i.e.* it is not an artifact. The full width at half maximum of the peak is 80 $ms = 1/4\ T_{\text{int}}$ and one can see a weak trace of the forcing of the flow at $\tau = \pm 1\ T_{\text{int}}$. The peak being at $\tau > 0$ translates to a_N initiating the change of $|\boldsymbol{v}|\times\omega_B$. Considering that $\omega_B = \boldsymbol{\omega}\cdot\boldsymbol{B} = \cos\theta\cdot|\boldsymbol{\omega}|$, only the quantities $|\boldsymbol{v}|$, $|\boldsymbol{\omega}|$ and $\cos\theta$ can cause to the displacement of the peak. Nevertheless, a possible origin of this displacement can be also a difference between the relative, $\boldsymbol{v}_{\text{rel}}$, and the absolute particle velocity $\boldsymbol{v}$.

[1] left: no restriction of the observation volume, middle and right: using only data within a box in the center with edge length $d = 12cm$ or $6cm$, respectively

Fig. 5a shows the auto correlation for these quantities as well as for a_N and $|\boldsymbol{\omega}|$. Surprisingly, $\cos\theta$, $|\boldsymbol{v}| \times \omega_B$ and ω_B fall onto each other. That is in agreement with the cross correlations shown in Fig. 5b: the cross correlations $R(a_N, \omega_B)$, $R(a_N, |\boldsymbol{v}| \times \omega_B)$ and $R(a_N, \cos\theta)$ fall onto each other, too. Surprisingly, the very strong and sharp correlation between $\cos\theta$ and $|\boldsymbol{v}| \times \omega_B$ shows that a change in $\cos\theta$ instantly affects the lift force $|\boldsymbol{v}| \times \omega_B$.

We further find that $|\boldsymbol{\omega}|$ has 2 time scales, one of the order of a few Kolmogorov time scales, τ_η, and one of order of the integral time scale, T_{int}. Similar behavior has been observed for the vorticity in jets Mazellier (2005). In addition, the shape of auto correlation function resembles a model proposed recently by Alain Pumir and Michael Wilkinson (Wilkinson & Pumir (2011)).

3. Concluding remarks

The clear preferential alignment and the conditioning the acceleration (force) on the angular velocity of the particle provides evidence for the lift effect, *i.e.* of a strong coupling between

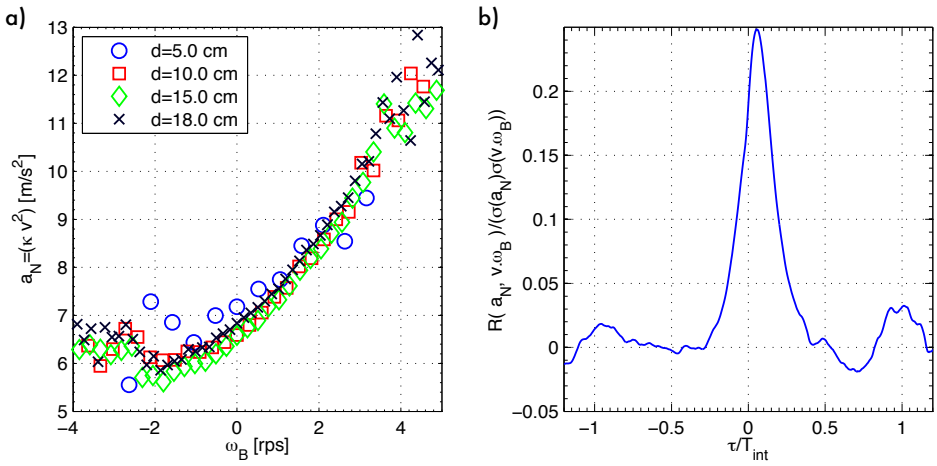

Figure 4. **a)** Normal acceleration, a_N, conditioned on the component of angular velocity parallel to the bi-normal Frenet vector for different box sizes d;
b) cross correlation between a_N and the lift force $|\boldsymbol{v}| \times \omega_B$

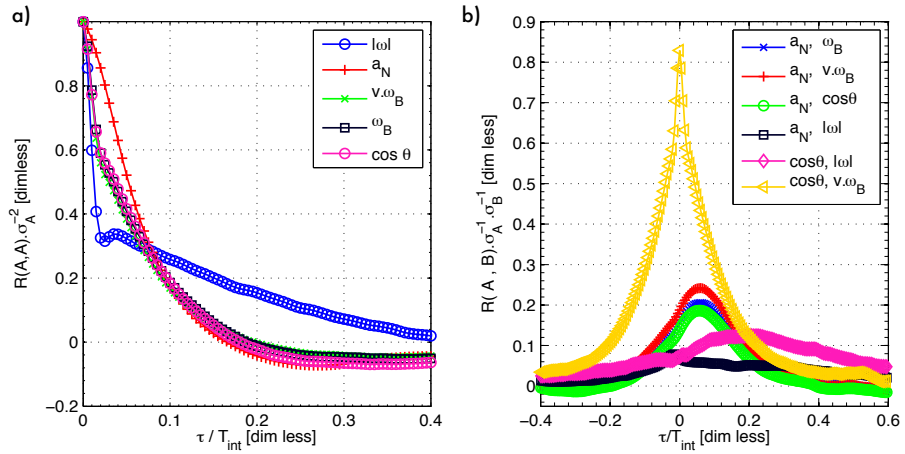

Figure 5. **a)** Auto-correlation of a_N, $|\boldsymbol{\omega}|$, $\cos\theta$, $|\boldsymbol{v}| \times \omega_B$ and ω_B **b)** Cross-correlations $R(a_N, |\boldsymbol{\omega}|)$, $R(a_N, \omega_B)$, $R(a_N, |\boldsymbol{v}| \times \omega_B)$, $R(a_N, \cos\theta)$, $R(\cos\theta, |\boldsymbol{\omega}|)$ and $R(\cos\theta, |\boldsymbol{v}| \times \omega_B)$

rotation and translation. The investigation of the auto and cross correlations found that the angle θ between $\boldsymbol{B}$ and $\boldsymbol{\omega}$ is strongly correlated with the lift force $|\boldsymbol{v}| \times \omega_B$ and that the normal acceleration, a_N, initiates a change in the lift force $|\boldsymbol{v}| \times \omega_B$. Further measurements are necessary to verify the latter observation is not due to a difference between the relative velocity and the measured absolute particle velocity.

The actual torque acting on the particle depends on the local structure of the flow, which remains to be determined, either experimentally Gibert *et al.* (2011), or numerically (*e.g.* Homann & Bec (2010); Naso & Prosperetti (2010)). A detailed study of the quantities studied here as a function of particle size and Reynolds number are ongoing and should yield important clues on the interaction between the turbulent flow and the particle. We are also working on a comparison of the model proposed by Wilkinson & Pumir (2011) to our measurements.

References

Auton, T R, Hunt, JCR & Prud'homme, M 1988 The force exerted on a body in inviscid unsteady non-uniform rotational flow. *J Fluid Mech* **197**, 241–257.

Gatignol, R 1983 Gatignol. *Journal de Mecanique Theorique et Appliquée* **2** (2), 143–160.

Gibert, M, Klein, S & Bodenschatz, E 2011 Flow around finite-size neutrally buoyant lagrangian particles in fully developed turbulence. In *Conference "Particles in turbulence"*.

Homann, H & Bec, J 2010 Finite-size effects in the dynamics of neutrally buoyant particles in turbulent flow. *J Fluid Mech* **651**, 81.

Loth, E & Dorgan, A. J 2009 An equation of motion for particles of finite reynolds number and size. *Environ Fluid Mech* **9** (2), 187–206.

Maxey, MR & Riley, JJ 1983 Equation of motion for a small rigid sphere in a nonuniform flow. *Physics of Fluids* **26**, 883.

Mazellier, Nicolas 2005 Dynamique spatio-temporelle du champ de vorticité en turbulence : mesures par corrélation acoustique dynamique. PhD thesis, Université Joseph Fourier - Grenoble.

Naso, A & Prosperetti, A 2010 The interaction between a solid particle and a turbulent flow. *New Journal of Physics* **12**, 033040.

Ouellette, N T, Xu, H, Bourgoin, M & Bodenschatz, E 2006 Small-scale anisotropy in lagrangian turbulence. *New Journal of Physics* **8**, 102.

Rastello, M, Marié, JL, Grosjean, N & Lance, M 2009 Drag and lift forces on interface-contaminated bubbles spinning in a rotating flow. *J Fluid Mech* **624**, 159.

Toschi, F & Bodenschatz, E 2009 Lagrangian properties of particles in turbulence. *Annual Review of Fluid Mechanics* **41** (1), 375–404.

van Nierop, EA, Luther, S, Bluemink, J J, Magnaudet, J, Prosperetti, A & Lohse, D 2007 Drag and lift forces on bubbles in a rotating flow. *J Fluid Mech* **571**, 439.

Wilkinson, M & Pumir, A 2011 Spherical Ornstein-Uhlenbeck processes. *arXiv* **physics.flu-dyn**.

Zimmermann, R, Gasteuil, Y, Bourgoin, M, Volk, R, Pumir, A & Pinton, J-F 2011*a* Rotational intermittency and turbulence induced lift experienced by large particles in a turbulent flow. *Phys. Rev. Lett.* **106** (15), 154501.

Zimmermann, R, Gasteuil, Y, Bourgoin, M, Volk, R, Pumir, A & Pinton, J-F 2011*b* Tracking the dynamics of translation and absolute orientation of a sphere in a turbulent flow. *Review of Scientific Instruments* **82** (3), 033906.